Historical perspective Probing the threshold of membrane damage and cytotoxicity effects induced by silica nanoparticles in Escherichia coli bacteria

Marion Mathelié-Guinlet, Laure Béven, Fabien Moroté, Daniel Moynet, Christine Grauby-Heywang, Ibtissem Gammoudi, Marie-Hélène Delville, Touria Cohen-Bouhacina

Historical perspective

Probing the threshold of membrane damage and cytotoxicity effects induced by silica nanoparticles in *Escherichia coli* bacteria

Marion Mathelié-Guinlet[a,b], Laure Béven[c], Fabien Moroté[a], Daniel Moynet[d], Christine Grauby-Heywang[a], Ibtissem Gammoudi[a,e], Marie-Hélène Delville[b,*], Touria Cohen-Bouhacina[a,e,**]

[a] *Univ. Bordeaux, CNRS, LOMA, UMR 5798, 351 cours de la Libération, 33400 Talence, France*
[b] *Univ. Bordeaux, CNRS, ICMCB, UPR 9048, 87 avenue du Dr Albert Schweitzer, 33608 Pessac, France*
[c] *Univ. Bordeaux, INRA, UMR 1332 Biologie du Fruit et Pathologie, 33140 Villenave-d'Ornon, France*
[d] *Univ. Bordeaux, INSERM U1035, 146 rue Léo Saignat, 33000 Bordeaux, France*
[e] *Cellule de transfert NanoPhyNov, ADERA, LOMA, 351 cours de la Libération, 33400 Talence, France*

Keywords:
E. coli
Silica nanoparticles
Membrane
Toxicity
AFM

A B S T R A C T

The engineering of nanomaterials, because of their specific properties, is increasingly being developed for commercial purposes over the past decades, to enhance diagnosis, cosmetics properties as well as sensing efficiency. However, the understanding of their fate and thus their interactions at the cellular level with bio-organisms remains elusive. Here, we investigate the size- and charge-dependence of the damages induced by silica nanoparticles (SiO_2-NPs) on Gram-negative *Escherichia coli* bacteria. We show and quantify the existence of a NPs size threshold discriminating toxic and inert SiO_2-NPs with a critical particle diameter (Φ_c) in the range 50nm–80nm. This particular threshold is identified at both the micrometer scale *via* viability tests through Colony Forming Units (CFU) counting, and the nanometer scale *via* atomic force microscopy (AFM). At this nanometer scale, AFM emphasizes the interaction between the cell membrane and SiO_2-NPs from both topographic and mechanical points of view. For SiO_2-NPs with $\Phi > \Phi_c$ no change in *E. coli* morphology nor its outer membrane (OM) organization is observed unless the NPs are positively charged in which case reorganization and disruption of the OM are detected. Conversely, when $\Phi < \Phi_c$, *E. coli* exhibit unusual spherical shapes, partial collapse, even lysis, and OM reorganization.

1. Introduction

For the past decades, nanotechnologies field has experienced a fast and growing development in many areas (microelectronics, medical imaging, cosmetics…) because of the specific physico chemical properties of nanoparticles (NPs). Though, this enthusiasm began to be questioned as NPs might put environmental safety and human health at risk by interacting with biological systems and affecting their behavior at the cellular level [1 7]. The diversity of NPs in terms of composition, shape and size/diameter (Φ) challenges politicians for regulating their safe use, and scientists for understanding how they interact with living organisms [8,9]. Such regulation and understanding are, though, necessary for the safe development of various applications like diagnosis in medicine [10 12], smart textiles conception [13,14], environmental treatments and detection sensors [15,16].

Among widely used biological systems, *Escherichia coli* is the most thoroughly studied species of bacteria. Ubiquitous in the environment, *E. coli* are Gram negative bacteria which, along with the cytoplasmic membrane and a peptidoglycan layer, possess an outer membrane (OM) composed of a phospholipid bilayer, containing lipopolysaccharide (LPS) molecules and proteins [17]. Potential human infections and diseases need to be considered as a consequence of exposure to several *E. coli* strains. The strain *E. coli* MRE 162 that we used in this work was first studied during the Lyme Bay trials in 1966 in order to mimic real biological attacks and to determine how United Kingdom (UK) populations could be at risk. Releasing massive amount of such bacteria, UK militaries reported chest and blood infections, caused by inhalation of *E. coli* MRE 162, especially in individuals highly susceptible to disease and exposed to contaminated clouds [18].

Studies on the antibacterial activity of NPs towards other *E. coli* strains showed that diverse metal oxides [19], iron [20] copper and silver [21] based nanomaterials exhibit a bactericidal activity. Major

* Corresponding author.
** Correspondence to: T. Cohen-Bouhacina, Univ. Bordeaux, CNRS, LOMA, UMR 5798, 351 cours de la Libération, 33400 Talence, France.
E-mail addresses: marie-helene.delville@icmcb.cnrs.fr (M.-H. Delville), touria.cohen-bouhacina@u-bordeaux.fr (T. Cohen-Bouhacina).

toxicity mechanisms include the disruption of the bacterial membrane integrity leading to the leakage of intracellular components [22], the production of reactive oxygen species (ROS) damaging bacterial con stituents [21] and/or the dissolution of NPs into their constituting ions interfering with the bacterial metabolism [23]. These mechanisms depend on multiple factors (composition, chemical functionalities, shape), especially the size and charge of NPs [29 33]. For instance, Beddoes et al. have presented an overview of in vivo and in vitro studies on human cells, and membrane models simulations, reporting that (i) small NPs (tens of nm) translocate very efficiently through the membrane causing cellular damage while large NPs (hundreds of nm) exhibit strong cellular uptake without toxicity; (ii) positively charged NPs disrupt membrane integrity and are more toxic than negatively charged NPs [8].

Because of their relatively low toxicity towards eukaryotic cells, their biocompatibility and their easy surface modifications, silica NPs (SiO_2 NPs) are good candidates for biomedical imaging, drug delivery, and biosensor applications [34,35]. Interestingly, SiO_2 NPs, not per se but functionalized with either photosensitizing molecules or antibiotics, or anchored to nanohybrid materials are promising both in bacterial detection [36] and antibacterial activity [37]. Despite this great potential, the interactions of non functionalized SiO_2 NPs with bacteria are not well documented in the literature. Most studies on toxicity of such NPs towards microorganisms rely on colorimetric methods or on Colony Forming Units (CFU) counting which allow the quantification of the minimum bactericidal concentration and the determination of the percentage of dead cells [38,39]. However, even if the death of cells is a key parameter, their behavior in the presence of bactericidal com pounds is also crucial to investigate and to understand the underlying toxicity mechanisms and to distinguish between the effects of different parameters such as NPs size and charge.

Some authors used transmission electron microscopy (TEM) to observe the morphological damages induced to *E. coli* cells by ZnO and Ag NPs [40,41]. Confocal Raman spectroscopy molecular inter pretation for such damages was also performed for GaN NPs interacting with different bacterial strains [22]. In this context, atomic force microscopy (AFM) is also another technique which provides comple mentary opportunities (i) to observe biological systems at a nanometer scale, both in air and in physiological environment, and (ii) to probe their nanomechanical properties in real time [42 44]. Under these conditions, AFM is thus a pertinent technique to analyze bacteria morphological and rheological damages induced by potentially anti bacterial agents, such as NPs, with details at the nanoscale.

In the present work, our main objectives were to better understand the process of interaction of SiO_2 NPs with *E. coli* MRE 162, for which, to our knowledge, it is the first study of exposure to NPs. We aimed at determining a potential size and charge threshold, for which SiO_2 NPs would be toxic towards *E. coli*. NPs of 100 nm in diameter and larger have been shown to exhibit similar behaviors so that the herein considered range (4 nm to 100 nm) will focus on all the opened questions about size dependent biotoxicity of NPs [45,46]. These SiO_2 NPs were characterized in terms of size distribution and aggrega tion state in solution. We first quantified the bacterial viability upon incubation with such particles. Then, we focused on how the presence of SiO_2 NPs of different sizes and charges disturbs the bacteria morphology and the mechanical properties of their membrane, by taking advantage of AFM in tapping mode and finally correlated these data with the viability results.

2. Results

2.1. Size and charge characterization of SiO_2 NPs

Dynamic Light Scattering (DLS) measurements (Table 1) revealed that, for the largest SiO_2 NPs^- ($\Phi \geq 50$ nm), the average hydrody namic diameter was larger than the primary particle sizes obtained by TEM. On the contrary, for the smallest SiO_2 NPs^- ($\Phi < 50$ nm), it was underestimated as compared to values provided by manufacturers and TEM. Size distributions, obtained by statistics on TEM clichés, suggest that all SiO_2 NPs are quite monodisperse (Fig. S1).

Table 1
Characterization of SiO_2-NPs, both commercial and home-made, by DLS and zeta potential measurements and statistics on TEM pictures.

Name	Diameter (nm)			Zeta potential (mV)
	Manufacturer	TEM	DLS	
SiO_2-NPs 4	4 (large distribution)	aggregated	3	53.3
SiO_2-NPs 10	10 ± 5	12 ± 4	7	
SiO_2-NPs 50	50 ± 10	53 ± 12	68	
SiO_2-NPs 80	Home made	81 ± 4	90	
SiO_2-NPs 100	100 ± 30	113 ± 11	124	
SiO_2-NPs^+ 100	Home made	94 ± 4	135	+ 45.4

Zeta potential measurements (Table 1) indicated that, as expected, bare SiO_2 NPs^- were highly negatively charged at pH 5.5 resulting in the stability of the suspensions and a minimal aggregation state for these NPs. After functionalization with APS, at pH 5.5, SiO_2 NPs exhibited, as expected, highly positive charges (SiO_2 NPs^+), also resulting in a good colloidal stability.

Thereafter, these well defined SiO_2 NPs were studied in interaction with *E. coli* cells (i) at the macroscopic level with viability tests and (ii) at the nanometer scale with AFM observations.

2.2. Effects of SiO_2 NPs^- on E. coli cells viability

The potential antibacterial effect of SiO_2 NPs^- was estimated by counting CFUs generated after treatment by a solution of NPs at a concentration of 1 g/L, on LB agar plates, and normalizing them with those of *E. coli* alone (OD = 0.01, control). Though most of such experiments required buffer solutions, ours were performed in ultra pure water for convenient reasons (AFM characterizations afterwards). No mortality is observed in this solvent (results not shown) in agreement with previous studies showing the strong resistance of *E. coli* in drastic environment, depending on pH and temperature for instance [47 49]. The development of CFUs is known to depend on two contributions: (i) the initial distribution of the bacteria in suspension and (ii) the toxicity of the environment, i.e. its capability, after potential treatment, to generate a CFU. Thus, the influence of the presence of SiO_2 NPs^- is investigated under these perspectives.

Under static conditions, two sets of behavior were observed: (i) SiO_2 NPs^- 100 had no detrimental effect on the bacteria, with a CFU number close to those of the control, while (ii) the presence of smaller SiO_2 NPs^- (4 nm to 80 nm) did induce an increase in these CFUs (Fig. 1a). In addition, the clustering state of *E. coli* cells upon SiO_2 NPs^- treatment was studied by dark field microscopy (see Fig. 1b for representative images). In controls, *E. coli* were present as isolated cells as well as small aggregates. The same organization was observed in the presence of SiO_2 NPs^- 80 and 100. By contrast, in the presence of SiO_2 NPs^- 4, 10 and 50, the number of isolated cells was increased. Such splitting of cells clusters is likely at the origin of the CFUs increase (Fig. 1c), interactions between such SiO_2 NPs^- and *E. coli* being stronger than cell cell interactions. Similar behaviors were observed for *E. coli* incubated with SiO_2 NPs^- during 24 h, suggesting that their full activity is reached in 2 h (Fig. S2).

However, this technique appears insufficient to probe any toxicity phenomena of SiO_2 NPs^- as they could combine, more or less, with splitting effects (Fig. 1c).

Consequently, AFM experiments were carried out to better under stand, visualize and characterize the type of interaction of SiO_2 NPs^- with *E. coli* and their potential deleterious effects.

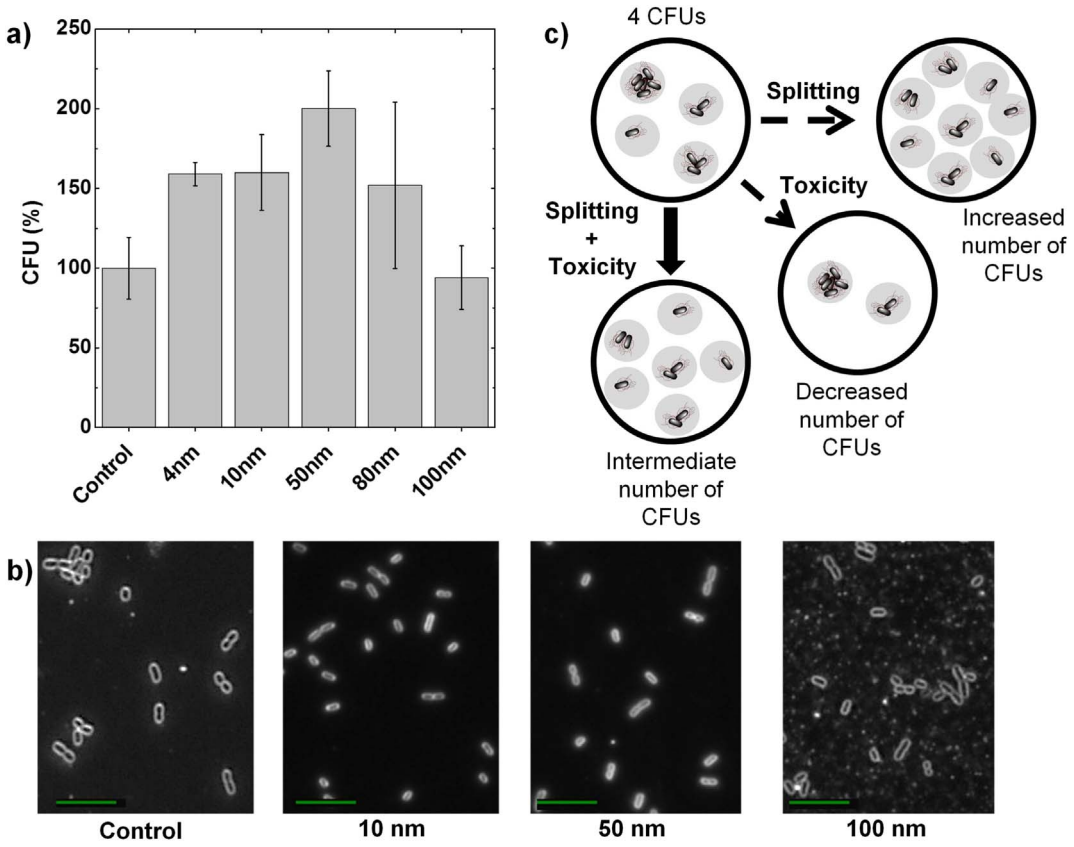

Fig. 1. a) Potential antibacterial activity of SiO_2-NPs (1 g/L) against *E. coli* cells (OD = 0.01). b) Optical microscopy (dark field) observations of representative samples, with and without SiO_2-NPs, revealing modifications in cells organization and morphology (scale bar: 10 μm). c) Scheme of the potentially entangled effects of SiO_2-NPs with $\Phi < \Phi_c$ and their consequences on CFUs.

2.3. Morphological characterization of *E. coli* bacteria by AFM

Before investigating their interactions with SiO_2 NPs, the morphology and the structure of *E. coli* cells alone were characterized. In air, *E. coli* bacteria exhibited a typical rod shape, convention name that is widely used for such bacteria [50] (Fig. 2a). *E. coli* length, width and height were estimated, on average, at 2.0 μm, 1.2 μm and 0.3 μm, respectively. Also, *E. coli* surface showed a "brain like" aspect not only from the morphology point of view (Fig. 2b) but also from the rheology point of view with nanodomains, referred as "ripples" thereafter (Fig. 2c). The nanodomains were on average 3.9 ± 1.5 nm in height and 39.9 ± 7.4 nm in width. This particular phase separation pattern is due to the presence of an outer membrane (OM) in Gram negative bacteria. Based on the AFM tip interactions with the sample, phase contrasts on *E. coli* stand for membrane constituents with either different mechanical properties or different molecular organizations: ripples on the one hand and inter ripples on the other hand.

Morphological and structural characteristics of *E. coli* membrane being characterized, its interactions with SiO_2 NPs are hereafter studied, under these perspectives.

2.4. AFM study of the damages induced by SiO_2 NPs^- on *E. coli* cells

The potential impacts of SiO_2 NPs on the morphology and structure of *E. coli* cells are discussed hereafter, in terms of size dependency. In order to efficiently observe these damages we had to control the quantity of added SiO_2 NPs so as to image both SiO_2 NPs and bacteria the SiO_2 NPs concentration was then reduced from 1 to 0.1 g/L.

When treated with SiO_2 NPs^- at a concentration of 0.1 g/L, *E. coli* cells were present on the substrate as isolated cells or aggregates, as in untreated samples. All SiO_2 NPs^- accumulate not only around and on bacteria but also on the substrate, as free isolated or aggregated particles (Fig. 3a b). Because of their higher stiffness, SiO_2 NPs appear as brighter zones than bacteria in phase images, which also show their respective distribution on the substrate (Fig. 3c d).

When exposed to SiO_2 NPs^- 80 and 100, *E. coli* cells remained rod shaped and displayed the same height as control cells (Fig. 4a b). By contrast, in the presence of SiO_2 NPs^- 4, 10 and 50, *E. coli* morphology evolved from rod like to more spherical shape with up to 50% decrease in their length (Fig. 4c e).

After exposure to large SiO_2 NPs^- 80 and 100, *E. coli* cells not only exhibited an unchanged global morphology but also an unmodified phase separation pattern of its envelop, which remained similar to that of healthy unexposed cells (Fig. 5a b and Fig. S3). As soon as smaller SiO_2 NPs^- (4, 10 and 50 nm) were used, strong detrimental cell membrane reorganizations were observed along with morphological changes. Indeed, the brain like structure of the OM of *E. coli* was completely altered as compared to the OM structure of unexposed cells (compare Fig. 5a,c and Fig. S3): the ripples nanodomains turned into island like structures and several areas in the OM even lack any regular organization. At this point, the reorganization might arise from either a (i) different molecular packing, i.e. the way molecules of the OM arrange themselves on the surface, or (ii) a different molecular conformation, i.e. the way molecules of the OM self orientate themselves at the air bacteria interface (condensed or fluid conformation).

SiO_2 NPs^- not only affect the organization of the OM but also its morphology. When $\Phi > 50$ nm, two behaviors were observed: either (i) SiO_2 NPs^- were deposited on bacteria or (ii) they were trapped in between two cells (Fig. S4). In the latter case, the ripples nanodomains adapt to the NP shape, changing their orientation around the particle to partially wrap it like a "cocoon" (Fig. 6). The wrapping ratio can change among cells, leaving the NP more or less apparent (compare Fig. 6 and

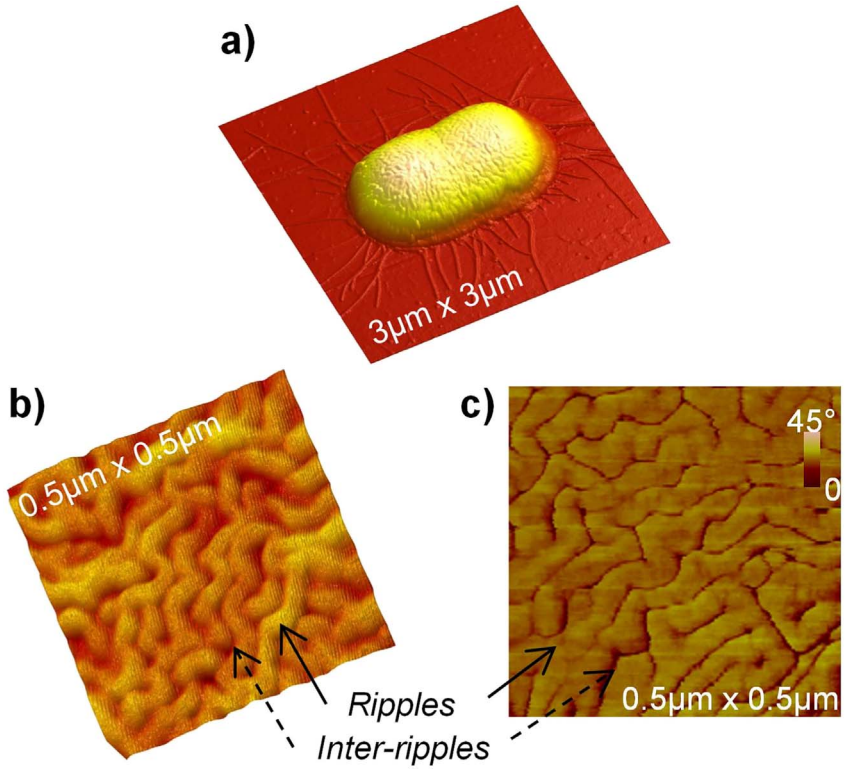

Fig. 2. Characterization of *E. coli* cells morphology and rheology by AFM observations. a) Height image of the rod bumped shape of a single cell. In some cases, despite their fragility, flagella and pili are still attached to the cell (white arrow). A zoom on its irregular surface reveals (b) a typical relief and (c) a phase separation pattern corresponding to the lamellae organization of the cell OM.

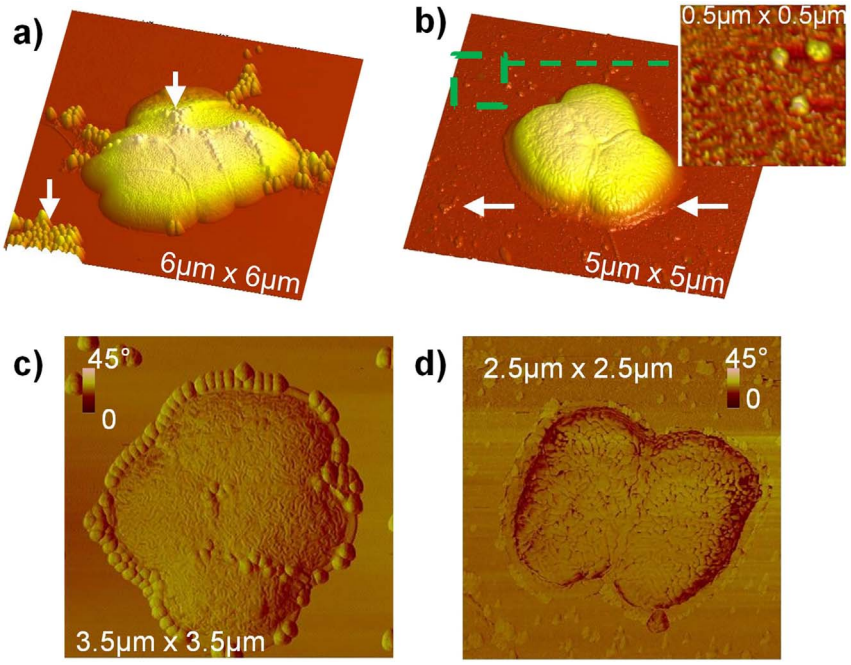

Fig. 3. Height (a-b) and phase (c-d) AFM images showing the organization of *E. coli* cells treated with (a) SiO_2-NPs 100, (b) SiO_2-NPs 4, (c) SiO_2-NPs 80 and (d) SiO_2-NPs 10. NPs are either deposited on and around cells or free on the substrate (white arrows).

Fig. S5).

When $\Phi \leq 50$ nm, membrane invaginations (pore like lesions), with well defined spherical edges, were observed randomly distributed on the bacterial surface (Fig. 7a). Even if cell dependent, their depth could reach down to few tens of nanometers (Fig. S6). Two behaviors are associated to these pore like lesions: either (i) the height profile is linked to a phase signature similar to the OM one or (ii) it exhibits a bump linked to a more repulsive signature similar to the NP one (Fig. 7b c).

We here demonstrated that drastic damages induced by SiO_2 NPs^- depend on a critical diameter ($50\text{ nm} < \Phi_c < 80\text{ nm}$) above which they were not observed anymore. The true question now is: do NPs induce any bactericidal effect?

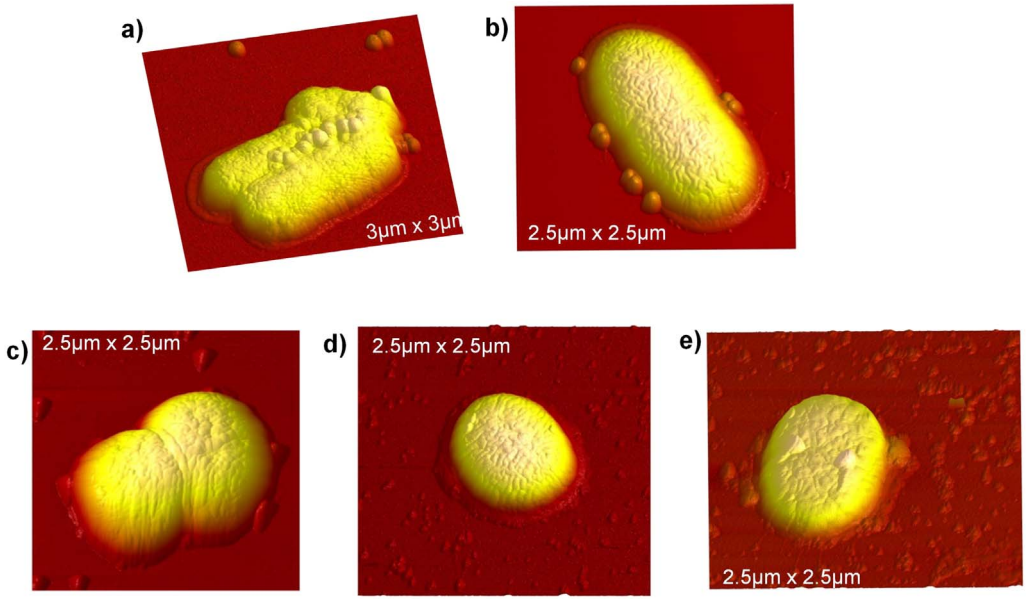

Fig. 4. Height AFM images, emphasizing no change in the morphology of *E. coli* cells after treatment with (a) SiO_2-NPs 100, (b) SiO_2-NPs 80, and aspect ratio modification after treatment with (c) SiO_2-NPs 50, (d) SiO_2-NPs 10 and (e) SiO_2-NPs 4.

2.5. Bactericidal effect of SiO_2 NPs^-

2.5.1. NPs size < critical diameter Φ_c

Besides membrane degradations, the incubation of *E. coli* cells with SiO_2 NPs^- 4, 10 and 50 resulted, in some cases, in the collapse of *E. coli* cells. It is either partial, resulting in a drastic decrease of the bacteria height, or total, and bacteria were drained from their cellular contents and no more exhibited well organized membrane structure (Fig. 8a,b). Moreover, debris were observed on the mica substrate in the vicinity of bacteria aggregates exposed to SiO_2 NPs^- 4 (Fig. 8c). Such fibrous materials, already observed as the result of cell surface perturbation [51], are indicative of cellular leakages. They can also correspond to membrane components such as LPS aggregates being expelled due to the stress induced by such NPs.

2.5.2. NPs size > critical diameter Φ_c

SiO_2 NPs^- 80 and 100 did not lead to any of these phenomena. In particular, *E. coli* cells suffered from no leakage of their intracellular compounds.

2.6. SiO_2 NPs charge effect on E. coli cells

To decorrelate between size and charge effects on the interaction between SiO_2 NPs and *E. coli*, the influence of SiO_2 NPs^+ 100 (> Φ_c) is

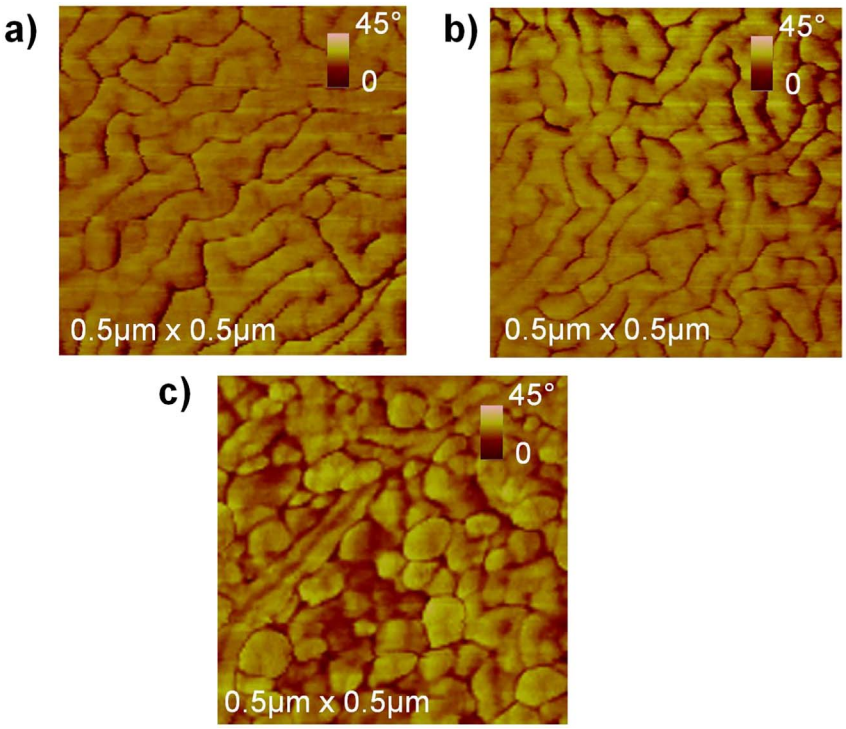

Fig. 5. AFM phase images of the OM features of *E. coli* cells (a) alone and incubated with (b) SiO_2-NPs 100 and (c) SiO_2-NPs 4 for which a transition in the ripples structures occurs.

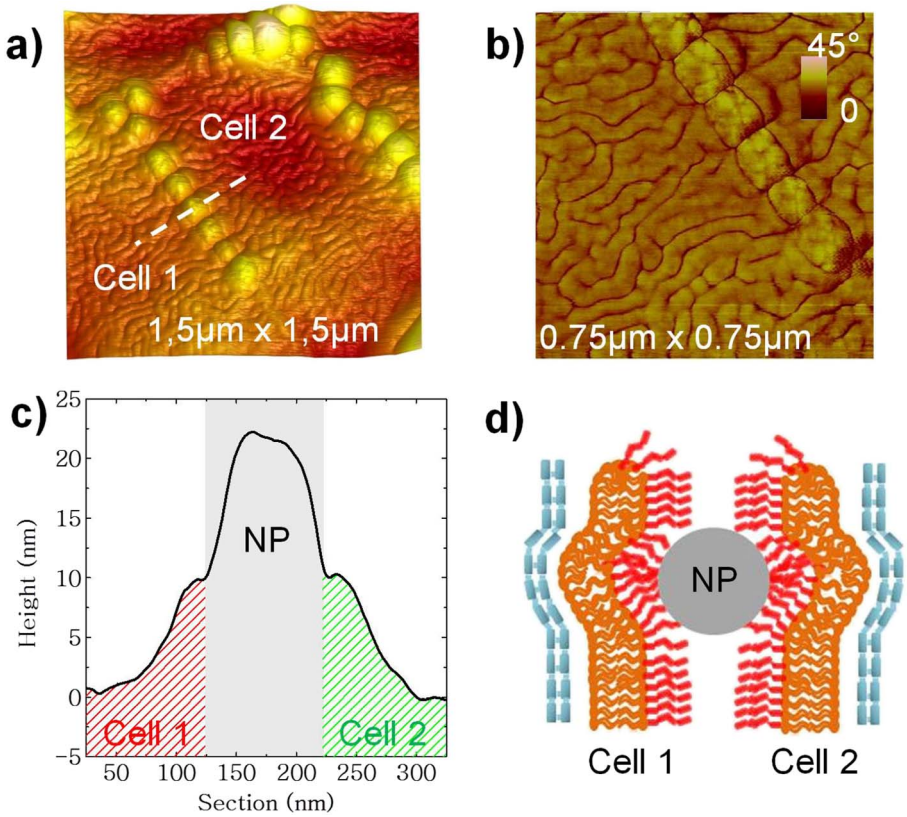

Fig. 6. a) Height AFM image showing the wrapping of SiO_2-NPs 100 in between two neighbor cells. b) A closer view of this phenomenon in phase image. c) Profile section of a SiO_2-NPs 100 showed by the dashed line in (a). d) Proposed scheme of the OM deformation, leading to the formation of a "cocoon" around the NP.

now investigated.

SiO_2 NPs^+ 100 did not affect the CFUs, as for SiO_2 NPs^- 100. However, AFM observations emphasized the aggregation between such positive NPs and *E. coli*. Indeed, unlike SiO_2 NPs^- 100, SiO_2 NPs^+ 100 tended to exclusively accumulate and stick to, around and on bacteria, none being observed as free isolated or aggregated particles on the substrate (compare Fig. 3 and Fig. 9a). This emphasizes the privileged electrostatic affinity between SiO_2 NPs^+ and the negatively charged surface of *E. coli*, as confirmed by zeta potential measurements.

Furthermore, modifying the charge of SiO_2 NPs 100 did not induce any change in *E. coli* rod shape morphology (Fig. 9b) nor in its OM ripples structure (Fig. 9c). However, unlike SiO_2 NPs^- 100 which did not lead to any membrane degradations, SiO_2 NPs^+ 100 induced drastic damages including the formation of (i) extra membrane aggregates and (ii) membrane invaginations. In the first case, aggregates with heights ranging from 4 to 15 nm surrounded cells (Fig. 10a b). In the second case, pore like lesions, similar to those observed with SiO_2 NPs^- smaller than Φ_c, exhibited a depth of few tens of nanometer, which are not correlated to the NP size (Fig. 10c d).

3. Discussion

This work is the first study of exposure to NPs of the strain *E. coli* MRE 162, which was used, during the 70's, for military purposes. Although thought to be inoffensive, these *E. coli* were reported to cause diseases in highly susceptible individuals. This emphasizes the necessity of investigating on proper antibacterial agents (harmless for human cells) such as NPs, for commonly found bacteria like *E. coli*.

Former studies on the toxicity of SiO_2 NPs present contradictory results not only because of different methodologies but also because they do not necessarily address the same size nor the same surface state of SiO_2 NPs, without explicitly mentioning these parameters in some cases. It is thus difficult to compare these results and to potentially demonstrate a size and charge effect tendency. In addition, despite a well known dose dependent cytotoxicity of antibacterial agents such as NPs [52], these studies differ in terms of concentration: *E. coli* growth inhibition was reported for a dose exposure of 2.0 g/L [38,53] while, in another study, a concentration as low as 0.2 g/L was inefficient [54].

Consequently, we undertook a systematic approach of this issue. We report herein (i) the potential antibacterial activity of SiO_2 NPs^-, with diameters varying from 4 to 100 nm, and (ii) the influence of the surface charge for the largest SiO_2 NPs (SiO_2 NPs^+ 100) on *E. coli* cells. Based on previous studies and submitted to AFM observation conditions (to correctly visualize both NPs and bacteria), toxicity tests were performed, under static conditions, after a 2 h incubation with NPs at a concentration of 0.1 g/L. Their toxicity was rationalized with regards to their size and charge effects.

Viability experiments revealed the existence of a NP size threshold, $50\ nm < \Phi_c < 80\ nm$. Above Φ_c, SiO_2 NPs^- had no influence on CFUs nor on the organization of *E. coli* population. Below Φ_c, SiO_2 NPs^- induced an increase in CFUs associated to the easier separation of the initial cell clusters. This phenomenon is not due to an improved ability of cells to divide but rather to the capacity of these SiO_2 NPs^-, despite their negative charge, to interact with the LPS layer of the bacteria OM, probably through hydrogen bonding with the LPS hydroxyl groups. These interactions are likely stronger than cell cell ones as they could break down cells clusters. To the best of our knowledge, this splitting effect has never been reported nor correlated to a size dependent action of NPs on cells. Former studies only described the size effect of NPs in terms of CFUs decrease always related to viability losses: for instance, the antibacterial activity decreases with an increase of the size of TiO_2 [31] and Ag [55] NPs. We, here, emphasized that CFUs counting is definitely insufficient by itself to probe toxicity phenomena since it reflects a competition between (i) the number of isolated cells, increased by splitting effects and (ii) the number of viable cells, decreased by potential antibacterial

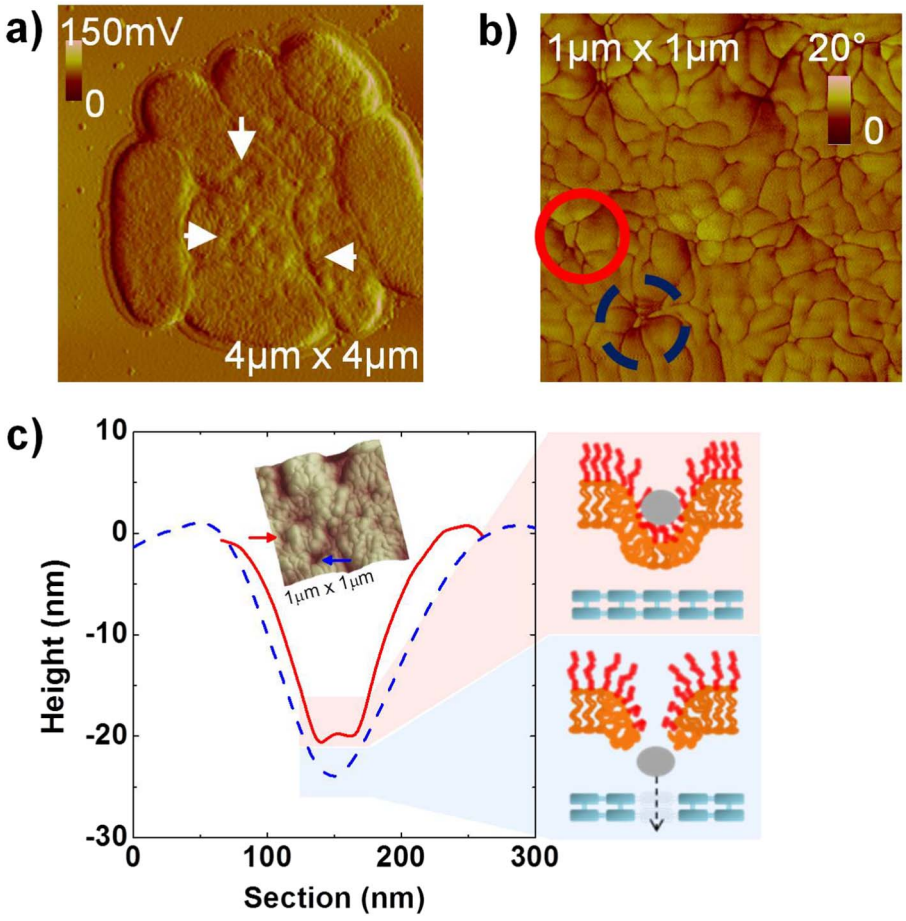

Fig. 7. a) AFM amplitude image showing membrane invaginations (white arrows) when *E. coli* cells are exposed to SiO_2-NPs 4. b) AFM phase image of a closer view of membrane invaginations with SiO_2-NPs 50 and (c) corresponding height profiles of the pore-like lesions pointed by red and blue lines in (b). Proposed scheme of the OM deformation is also shown in (c). (For interpretation of the references to colour in this figure legend, the reader is referred to the web version of this article.)

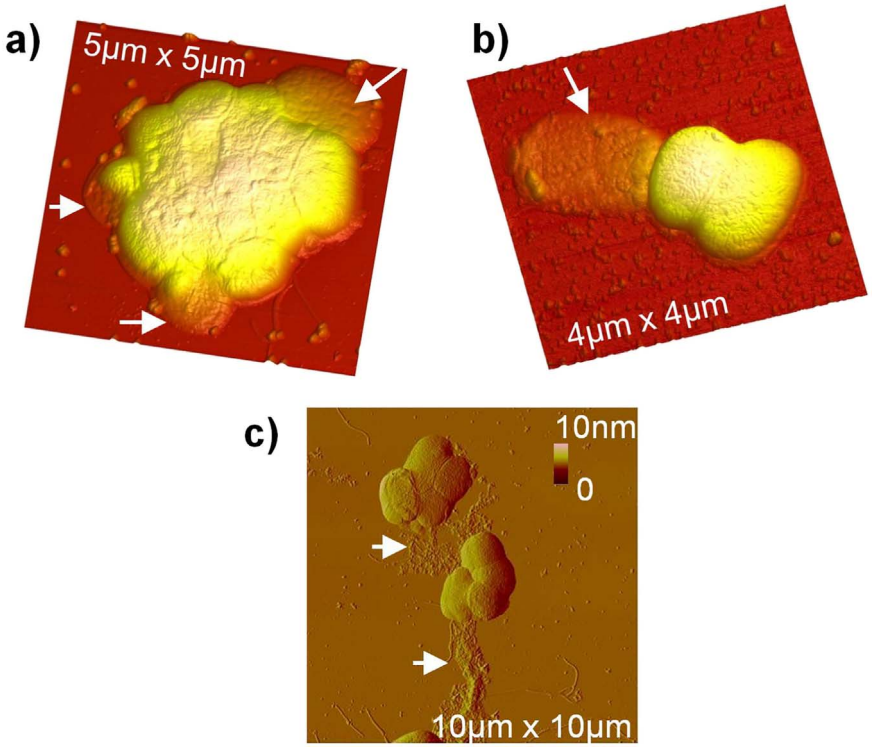

Fig. 8. Bactericidal effects of SiO_2-NPs with $\Phi < \Phi_c$ against *E. coli* cells. AFM height images of partially and totally collapsed cells when interacting with (a) SiO_2-NPs 50 and (b) SiO_2-NPs 10. c) AFM amplitude image showing debris due to bacteria lysis on the substrate when *E. coli* cells interact with SiO_2-NPs 4. Damages are indicated by full arrows.

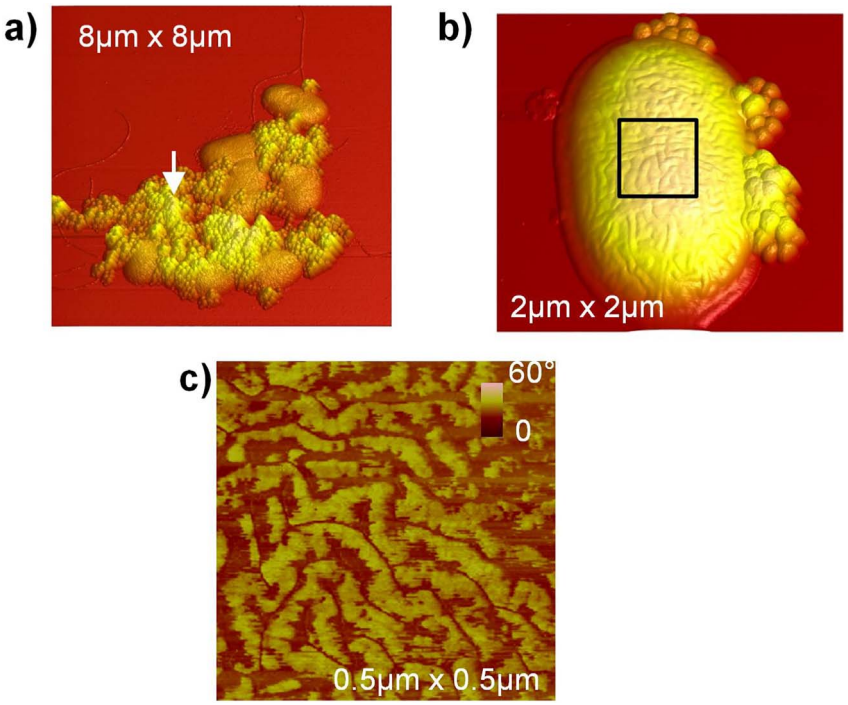

Fig. 9. a) AFM height images of *E. coli* cells population with SiO_2-NPs^+ 100, aggregated on cells (white arrow). AFM height (b) and phase (c) images of *E. coli* incubated with SiO_2-NPs^+ 100 showing its unchanged morphology and OM structure.

activity (Fig. 2c).

From this point of view, AFM proved to provide complementary and necessary information, at the cellular level, on the NPs size dependent antibacterial activity. Firstly, it emphasized the particular ultrastructure present on healthy *E.coli*'s surface. This "brain like" organization, here called ripples, is attributed to the conformation of LPS molecules in the OM [56]. Then, AFM observations confirmed, at the cellular level, the existence of a NPs size threshold, 50 nm $< \Phi_c <$ 80 nm. On the one hand, SiO_2 NPs^- larger than Φ_c do not induce any particular damage on the overall morphology of *E. coli* nor on its OM structure.

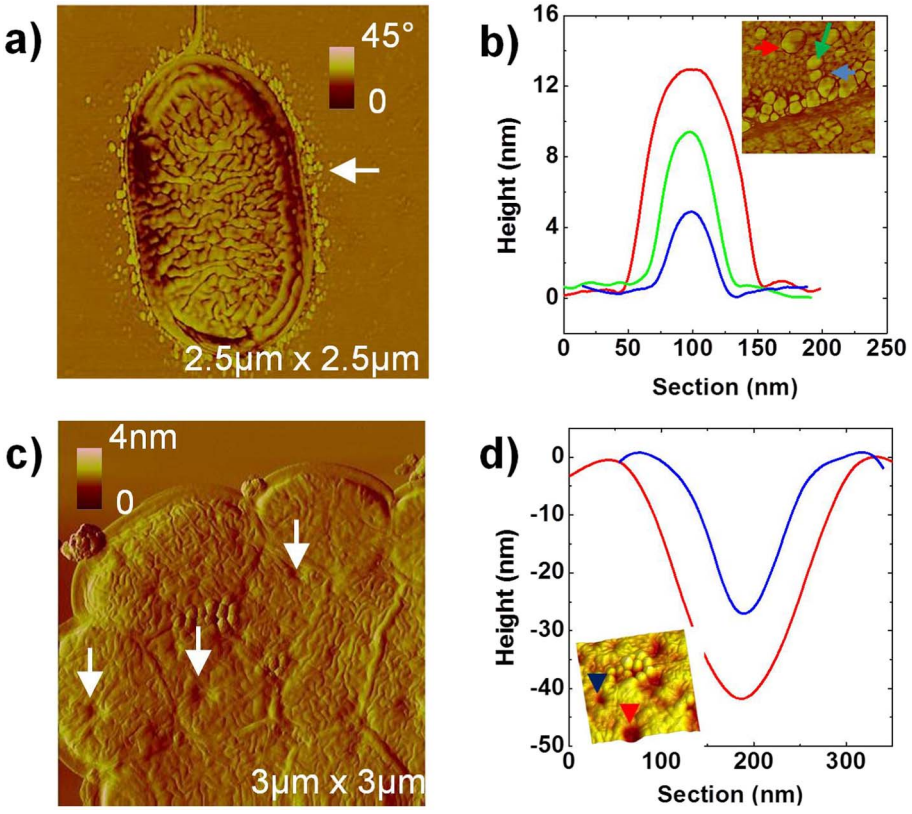

Fig. 10. *E. coli* membrane damages induced by SiO_2-NPs^+ 100, observed on AFM phase (a) and amplitude (c) images, and pointed by full arrows. a) Formation of extra-aggregates, with (b) height profiles representative of diverse aggregates. c) Formation of membrane invaginations with (d) height profiles representative of diverse invaginations.

Noteworthy is the partial wrapping observed for these NPs trapped in between cells (Fig. 6c). A balance between adhesion and free energies is here assumed for the NP not to translocate through cells, as already observed by Livadaru and Kovalenko in a statistical mechanical approach of membrane invaginations [57]. On the other hand, SiO_2 NPs^- smaller than Φ_c strongly disturb *E. coli* cells. The pore like lesions observed are deep enough, as compared to the OM thickness (around 8 nm), for these SiO_2 NPs^- to (i) disrupt this OM and induce its invagination or piercing and even to (ii) damage the underlying peptidoglycan layer (Fig. 7c) which is involved not only in cell division processes but also in the preservation of the cell wall uniformity and cell shape. Permeabilization of this layer is also reinforced by the more spherical shape of bacteria. Such invaginations were reported in antibiotic (penicillin and amoxicillin) treatment of *E. coli*, interfering with enzymes involved in the peptidoglycan synthesis [58]. In addition, SiO_2 NPs^- smaller than Φ_c induce a reorganization in *E. coli*'s OM structure from a ripples pattern to more compact and rounded aggregates, typical of weakened bacteria [56]. This transition might arise from (i) the spatial reorganization of the LPS molecules from a ripples structure to an aggregated one or (ii) from the transition in their molecular conformation from an extended to a more condensed one. In both cases, this transition is in agreement with the polymer like behavior [59] of LPS when undergoing an external pressure [60]. It is likely due to small SiO_2 NPs^- interfering in the core of the OM and forcing the molecules to reorganize as compression does in the case of Langmuir monolayer experiments (Fig. S3) [60]. It is not excluded either that a strong hydrogen bonding between these SiO_2 NPs^- and the multiple hydroxyls groups of LPS molecules does play a role in this disorganization. It induces a break in the crystalline organization of LPS and thus the loss of the brain like structure, this process being much easier with smaller NPs. At some point, especially for the 4 and 10 nm sizes, NPs might penetrate in the grooves of the LPS layer. Finally, observed lysis and consequent leakage of intracellular components, could occur through these pore like lesions or through the complete and direct destruction of the cell inner membrane. Indeed, cell lysis suggests that, when SiO_2 NPs^- reach the peptidoglycan layer, they are internalized and translocated, and reach the inner membrane leading to potential toxicity. For cells remaining alive (healthy appearance), SiO_2 NPs^- might be trapped outside the peptidoglycan layer protecting the inner membrane and thus the cell integrity. Considering these damages, SiO_2 NPs^- smaller than Φ_c have similar effects as some antimicrobial peptides following the “carpet model” [61,62].

Independently of their sizes, the positive surface charge of SiO_2 NPs generates strong attractive electrostatic interactions with negatively charged *E. coli* bacteria. This affinity appears to favor antibacterial activity of SiO_2 NPs. Indeed, SiO_2 NPs^+ 100 lead to drastic membrane invaginations, similar to those observed with SiO_2 NPs^- smaller than Φ_c and blebbing phenomenon. As $\Phi > \Phi_c$, the size influence is, here, ruled out, implying a different mechanism for such damages, probably a consequence of the electrostatic field induced by SiO_2 NPs^+. This surface charge dependent toxicity confirms previous studies on silver NPs either bare or coated [30,63].

4. Conclusion

We have demonstrated the size and charge dependent toxicity of SiO_2 NPs towards *E. coli* bacteria, through a systematic approach. Cells were exposed to commercial and home made SiO_2 NPs with different sizes (4, 10, 50, 80 and 100 nm), either bare (SiO_2 NPs^-) or functionalized (SiO_2 NPs^+) and their toxicity emphasized by viability tests and AFM observations. We demonstrated the existence of a critical diameter, $50\,nm < \Phi_c < 80\,nm$, under which cell damages were observed: OM invaginations and reorganization (from ripples for healthy cells to aggregates for weakened and damaged ones). We reported, for the first time, the splitting effects of these SiO_2 NPs^- on cells and its potential interaction with toxicity phenomena. We also showed that SiO_2 NPs larger than Φ_c did not affect *E. coli* cells unless they were positively charged, SiO_2 NPs^+ 100 inducing similar damage as the smallest negative SiO_2 NPs^-. Finally, the particular membrane reorganization emphasized the importance of LPS structure in *E. coli* in the resistance to external stress and the need for further studies on its nanomechanical properties and its interaction with NPs.

5. Materials and methods

For convenient reasons, we will use thereafter short names for all used NPs. For instance, negatively charged silica NPs of 4 nm in diameter will stand as SiO_2 NPs^- 4. Similar expressions will be used for all NPs.

5.1. Materials

Commercial SiO_2 NPs^- 10, 50 and 100 were purchased from Biovalley (Marne la Vallée, France) and SiO_2 NPs^- 4 from Alfa Aesar (Schiltigheim, France). Gram negative *E. coli* bacteria (MRE 162 strain) were a kind gift from the *Centre d'Etudes du Bouchet, DGA* (Direction Générale de l'Armement, France). Mica, purchased from Electron Microscopy Sciences (Hatfield, United States), was used as support for all AFM measurements. Luria Broth (LB) medium was used as nutritive medium and purchased from Fisher Scientific (Waltham, Massachusetts, United States). L Arginine and tetraethylorthosilicate (TEOS), used for silica seeds synthesis, were purchased from Sigma Aldrich (Saint Louis, Missouri, United States) as well as aminopropyl triethoxysilane (APS), used for NPs functionalization. Ethanol and ammonium hydroxide, used for SiO_2 NPs growth, were also purchased from Sigma Aldrich. Millipore ultrapure water (pH 5.5, resistivity > 18.2 MΩ cm) was used for NPs cleaning and bacteria suspensions preparation.

5.2. Preparation and characterization of SiO_2 NPs solutions

To obtain a large range of NPs sizes, we used both commercial and home synthesized SiO_2 NPs. Home synthesis was also used to functionalize the negatively charged NPs (SiO_2 NPs^-) and get a positive surface charge (SiO_2 NPs^+).

Commercial SiO_2 NPs^- were centrifuged three times at 9000*g* for 45 min (20 min were enough for SiO_2 NPs^- 100), cleaned and redispersed in ultrapure water. SiO_2 NPs^- were then placed in a sonication bath for approximately 1 h to ensure minimal aggregation in the solution.

Synthesis of home made SiO_2 NPs^- was carried out following synthesis developed by Hartlen et al. [64]. The first step consisted in synthesizing SiO_2 seeds. 100 mL of a 6 mM L arginine water solution was introduced in a vial at 60 °C, under magnetic stirring (150 rpm). After temperature stabilisation, 10 mL of TEOS were slowly added so as to respect the interface. Seeds of about 30 nm in diameter were obtained after complete consumption of TEOS. The second step consisted in the growth of these seeds. Typically, 10 mL of SiO_2 seeds were introduced in a mixture of 455 mL of ethanol and 35 mL of ammonium hydroxide in water solution ($[NH_3] = 1$ M), under stirring (700 rpm). TEOS was then introduced in the amount calculated to get the targeted diameter, at a rate of 0.5 mL/h [65]. Surface modification was performed by adding APS (six equivalents assuming a rate of 2 3 μmol/m^2 of active OH groups at the surface of the silica particles) to the SiO_2 NPs^- solution; the mixture was then stirred for 48 h in a water bath at room temperature, and then for 2 h at 100 °C. Final SiO_2 NPs^+ were washed using ultrapure water and ethanol and 3 cycles of centrifugation (13,000 rpm for 20 min.)

Dynamic Light Scattering (DLS) experiments were carried out on a Malvern Zetasizer Nano ZS setup (Orsay, France) to determine the size and polydispersity of NPs. This method provides information on both the hydrodynamic diameter of the SiO_2 NPs in solution and their

polydispersity. Transmission Electron Microscopy (TEM) with a JEOL JEM 1400 Plus and AFM observations were also used to investigate not only the size and morphology of SiO_2 NPs but also their organization on a substrate. Consequently, while TEM images give the silica NPs diameter (i.e. its core), DLS measurements give the hydrodynamic diameter of the NPs including the first sphere of coordination of the solvent. Zeta potential measurements were carried out on a Wallis Zeta potential analyzer from Cordouan (Pessac, France). For these three characterizations, SiO_2 NPs were suspended in ultrapure water to obtain a final concentration of 0.1 g/L and sonicated before any experiments.

5.3. Bactericidal susceptibility test

A fresh *E. coli* culture was obtained by inoculating 50 mL of LB medium with 250 µL of an overnight culture. The bacterial growth was followed by measuring the optical density (OD) at 600 nm, using a Helios gamma spectrophotometer (Thermo Scientific), until it reached 0.60. The suspension was further centrifuged (8000 rpm for 10 min. at 4 °C), and the cell pellet was re diluted in ultrapure water to obtain an OD of 0.01. Finally, NPs were introduced in the suspension at the desired concentration (1 g/L) and left to interact for 2 h, under static conditions, at room temperature. At the end of the incubation period, ten fold serial dilutions in ultrapure and sterile water of the suspensions were made and 100 µL of each dilution were spread onto LB agar plates. Bactericidal effects were evaluated by counting the number of colonies (CFU for colony forming units) developed on plates after 16 h at 37 °C. Average values of three independent experiments are reported there after.

5.4. Dark field microscopy observations

For dark field microscopy observations, *E. coli* cells were grown in LB medium until the culture reached an OD = 0.60 at 600 nm. The bacterial cells were centrifuged (8000 rpm for 10 min at 4 °C) and re suspended in ultrapure, sterile water to obtain an OD = 0.60 at 600 nm before being incubated in the presence of the different NPs at 1 g/L for 2 h at room temperature under static conditions. A microscope Eclipse Ni (Nikon) equipped with a dark field condenser (oil 1.463 1.20) and an objective Achromat 40 ×/0.65 both from Nikon was used for dark field image acquisition. Images were acquired with a Nikon DS Qi1Mc camera and NIS Elements software. Representative images are provided thereafter.

5.5. Preparation of NPs E. coli suspensions for AFM experiments

E. coli cells were grown on LB agar plates and incubated for 16 h at 37 °C. After scraping, bacteria were suspended in ultrapure water and their concentration was adjusted to 10^6 cells/mL. An equivalent volume of *E. coli* cells and SiO_2 NPs suspensions at a concentration of 0.1 g/L, were mixed and gently manually shaken (4 times every 20 min), then left to interact at room temperature for 2 h. Five microliters of each mixed suspension was deposited on freshly cleaved mica, left to dry in a desiccator and imaged by AFM the following day.

5.6. AFM experiments

Briefly, AFM consists of a cantilever with a nanoprobe at its end which, along with a piezo scanner, scans the sample surface. In close proximity, small (attractive and repulsive) forces between the probe and the surface lead to the deflection of the cantilever, which is recorded. This technique gives information on morphological and mechanical properties (adhesion, visco elasticity) of a surface, at the nanometer level. In this work, AFM experiments were carried out using a Bioscope II mounted on an IX71 Olympus inverted optical microscope operating with the NanoScope V controller and also with a Multimode AFM (Veeco Brucker, Santa Barbara, USA).

Though, imaging in liquid is preferred for cells hydration, air conditions were privileged for a better resolution [42,66] (due to tip bacteria interactions), notably on the topographical and nanomechani cal contrasts on the surface structure of bacteria. It also allows to work in dynamic tapping mode and, consequently, to take advantage of the harmonic oscillator behavior of the cantilever. Thus, very small forces were used, preventing any damages to the samples. Tapping mode images were obtained with commercial cantilevers with a spring constant around 40 N/m, at a scan rate of 0.5 to 1.0 Hz and with a resolution of 512 × 512 pixels. For each experiment, height, amplitude and trace phase images were recorded. Height images stand for topographical relief of the sample. Phase images show the phase difference between exciting and response signals, arising from the sample nanomechanical properties. Thus, they are linked to (i) dissipa tion processes between the tip and the sample and (ii) surface hardness. For instance, a homogenous surface (composition and organization) will not show any significant contrast in phase. Amplitude images (error signal) provide additional information on the topography and morphology of very fine details which might be saturated in height images.

Hereafter, samples were observed, in tapping mode, in the day following their preparation to prevent any interference, like ageing of *E. coli* biofilm [56], with the potential damage caused by SiO_2 NPs. Different areas were systematically scanned and images shown there after are representative of the cells in a given set of colonies and of all the tested samples.

Acknowledgments

The authors thank the Région Aquitaine and CNRS (France) for supporting this work through the equipment of the NanoSpectroImagerie (NSI LOMA) platform used in this work (CPER COLA2). They are grateful to the Direction Générale de l'Armement (DGA, Ministère de la Défense France, grant number : 2014017) and the Région Aquitaine (France) for their financial support through the Ph.D. grant of M. Mathelié Guinlet. Finally, authors thank NSI LOMA plat form for technical help and J.P Chapel for its helpful advises and discussions about DLS measurements.

Appendix A. Supplementary data

Supplementary data to this article can be found online at http://dx.doi.org/10.1016/j.cis.2017.04.012.

References

[1] Srivastava V, Gusain D, Sharma YC. Critical review on the toxicity of some widely used engineered nanoparticles. Ind Eng Chem Res 2015;54:6209–33. http://dx.doi.org/10.1021/acs.iecr.5b01610.
[2] Buzea C, Pacheco II, Robbie K. Nanomaterials and nanoparticles: sources and toxicity. Biointerphases 2007;2:MR17. http://dx.doi.org/10.1116/1.2815690.
[3] Kahru A, Ivask A. Mapping the dawn of nanoecotoxicological research. Acc Chem Res 2013;46:823–33. http://dx.doi.org/10.1021/ar3000212.
[4] Nel A, Xia T, Mädler L, Li N. Toxic potential of materials at the nanolevel. Science 2006;311:622–7.
[5] Oberdörster G, Oberdörster E, Oberdörster J. Nanotoxicology: an emerging discipline evolving from studies of ultrafine particles. Environ Health Perspect 2005;113:823–39. http://dx.doi.org/10.1289/ehp.7339.
[6] Lewinski N, Colvin V, Drezek R. Cytotoxicity of nanoparticles. Small 2008;4:26–49. http://dx.doi.org/10.1002/smll.200700595.
[7] Djurišić AB, Leung YH, Ng A, Xu XY, Lee PK, Degger N. Toxicity of metal oxide nanoparticles: mechanisms, characterization, and avoiding experimental artefacts. Small 2015;11:26–44.
[8] Beddoes CM, Case CP, Briscoe WH. Understanding nanoparticle cellular entry: a physicochemical perspective. Adv Colloid Interf Sci 2015;218:48–68. http://dx.doi.org/10.1016/j.cis.2015.01.007.
[9] Tolaymat TM, El Badawy AM, Genaidy A, Scheckel KG, Luxton TP, Suidan M. An evidence-based environmental perspective of manufactured silver nanoparticle in syntheses and applications: a systematic review and critical appraisal of peer-reviewed scientific papers. Sci Total Environ 2010;408:999–1006. http://dx.doi.

org/10.1016/j.scitotenv.2009.11.003.
[10] Farokhzad OC, Langer R. Impact of nanotechnology on drug delivery. ACS Nano 2009;3:16–20. http://dx.doi.org/10.1021/nn900002m.
[11] Duncan R, Gaspar R. Nanomedicine(s) under the microscope. Mol Pharm 2011;8:2101–41. http://dx.doi.org/10.1021/mp200394t.
[12] Das M, Duan W, Sahoo SK. Multifunctional nanoparticle–EpCAM aptamer bioconjugates: a paradigm for targeted drug delivery and imaging in cancer therapy. Nanomedicine Nanotechnol Biol Med 2015;11:379–89. http://dx.doi.org/10.1016/j.nano.2014.09.002.
[13] Dastjerdi R, Montazer M. A review on the application of inorganic nano-structured materials in the modification of textiles: focus on anti-microbial properties. Colloids Surf B Biointerfaces 2010;79:5–18. http://dx.doi.org/10.1016/j.colsurfb.2010.03.029.
[14] Yetisen AK, Qu H, Manbachi A, Butt H, Dokmeci MR, Hinestroza JP, et al. Nanotechnology in textiles. ACS Nano 2016. http://dx.doi.org/10.1021/acsnano.5b08176.
[15] Oliveira ON, Iost RM, Siqueira JR, Crespilho FN, Caseli L. Nanomaterials for diagnosis: challenges and applications in smart devices based on molecular recognition. ACS Appl Mater Interfaces 2014;6:14745–66. http://dx.doi.org/10.1021/am5015056.
[16] Sanvicens N, Pastells C, Pascual N, Marco M-P. Nanoparticle-based biosensors for detection of pathogenic bacteria. TrAC Trends Anal Chem 2009;28:1243–52. http://dx.doi.org/10.1016/j.trac.2009.08.002.
[17] Nikaido H. Molecular basis of bacterial outer membrane permeability revisited. Microbiol Mol Biol Rev 2003;67:593–656. http://dx.doi.org/10.1128/MMBR.67.4.593-656.2003.
[18] Spratt BG. Independent review of the possible health hazards of the large-scale release of bacteria during the dorset defence trials n.d.
[19] Kaweeteerawat C, Ivask A, Liu R, Zhang H, Chang CH, Low-Kam C, et al. Toxicity of metal oxide nanoparticles in *Escherichia coli* correlates with conduction band and hydration energies. Environ Sci Technol 2015;49:1105–12. http://dx.doi.org/10.1021/es504259s.
[20] Lee C, Kim JY, Lee WI, Nelson KL, Yoon J, Sedlak DL. Bactericidal effect of zero-valent iron nanoparticles on *Escherichia coli*. Environ Sci Technol 2008;42:4927–33. http://dx.doi.org/10.1021/es800408u.
[21] Yoon K-Y, Hoon Byeon J, Park J-H, Hwang J. Susceptibility constants of *Escherichia coli* and *Bacillus subtilis* to silver and copper nanoparticles. Sci Total Environ 2007;373:572–5. http://dx.doi.org/10.1016/j.scitotenv.2006.11.007.
[22] Sahoo P, Murthy PS, Dhara S, Venugopalan VP, Das A, Tyagi AK. Probing the cellular damage in bacteria induced by GaN nanoparticles using confocal laser Raman spectroscopy. J Nanopart Res 2013;15. http://dx.doi.org/10.1007/s11051-013-1841-9.
[23] Singh G, Joyce EM, Beddow J, Mason TJ, et al. Evaluation of antibacterial activity of ZnO nanoparticles coated sonochemically onto textile fabrics. J Microbiol Biotechnol Food Sci 2012;2:106–20.
[29] Goodman CM, McCusker CD, Yilmaz T, Rotello VM. Toxicity of gold nanoparticles functionalized with cationic and anionic side chains. Bioconjug Chem 2004;15:897–900. http://dx.doi.org/10.1021/bc049951i.
[30] Silva T, Pokhrel LR, Dubey B, Tolaymat TM, Maier KJ, Liu X. Particle size, surface charge and concentration dependent ecotoxicity of three organo-coated silver nanoparticles: comparison between general linear model-predicted and observed toxicity. Sci Total Environ 2014;468–469:968–76. http://dx.doi.org/10.1016/j.scitotenv.2013.09.006.
[31] Simon-Deckers A, Loo S, Mayne-L'hermite M, Herlin-Boime N, Menguy N, Reynaud C, et al. Size-, composition-and shape-dependent toxicological impact of metal oxide nanoparticles and carbon nanotubes toward bacteria. Environ Sci Technol 2009;43:8423–9.
[32] Xiao X, Montaño GA, Edwards TL, Allen A, Achyuthan KE, Polsky R, et al. Surface charge dependent nanoparticle disruption and deposition of lipid bilayer assemblies. Langmuir 2012;28:17396–403. http://dx.doi.org/10.1021/la303300b.
[33] Roiter Y, Ornatska M, Rammohan AR, Balakrishnan J, Heine DR, Minko S. Interaction of lipid membrane with nanostructured surfaces. Langmuir 2009;25:6287–99. http://dx.doi.org/10.1021/la900119a.
[34] Tan W, Wang K, He X, Zhao XJ, Drake T, Wang L, et al. Bionanotechnology based on silica nanoparticles. Med Res Rev 2004;24:621–38. http://dx.doi.org/10.1002/med.20003.
[35] Wang Y, Zhao Q, Han N, Bai L, Li J, Liu J, et al. Mesoporous silica nanoparticles in drug delivery and biomedical applications. Nanomedicine Nanotechnol Biol Med 2015;11:313–27. http://dx.doi.org/10.1016/j.nano.2014.09.014.
[36] Pham MT, Nguyen TV, Vu Thi TD, Nghiem Thi HL, Tong KT, Tran TT, et al. Synthesis, photophysical properties and application of dye doped water soluble silica-based nanoparticles to label bacteria *E. coli* O157:H7. Adv Nat Sci Nanosci Nanotechnol 2012;3:045013http://dx.doi.org/10.1088/2043-6262/3/4/045013.
[37] Liu T, Song X, Shen Y, Guo Z, Xue J, Wu H. Antibacterial mechanisms of silica/polydopamine/silver nanoparticles against gram positive and gram negative bacteria. Micro Nano Lett 2014;9:210–4. http://dx.doi.org/10.1049/mnl.2014.0014.
[38] Adams LK, Lyon DY, Alvarez PJJ. Comparative eco-toxicity of nanoscale TiO_2, SiO_2, and ZnO water suspensions. Water Res 2006;40:3527–32. http://dx.doi.org/10.1016/j.watres.2006.08.004.
[39] Lewinski N, Colvin V, Drezek R. Cytotoxicity of nanoparticles. Small 2008;4:26–49. http://dx.doi.org/10.1002/smll.200700595.
[40] Brayner R, Ferrari-Iliou R, Brivois N, Djediat S, Benedetti MF, Fiévet F. Toxicological impact studies based on *Escherichia coli* bacteria in ultrafine ZnO nanoparticles colloidal medium. Nano Lett 2006;6:866–70. http://dx.doi.org/10.1021/nl052326h.
[41] Sondi I, Salopek-Sondi B. Silver nanoparticles as antimicrobial agent: a case study on *E. coli* as a model for Gram-negative bacteria. J Colloid Interface Sci 2004;275:177–82. http://dx.doi.org/10.1016/j.jcis.2004.02.012.
[42] Bolshakova AV, Kiselyova OI, Yaminsky IV. Microbial surfaces investigated using atomic force microscopy. Biotechnol Prog 2004;20:1615–22. http://dx.doi.org/10.1021/bp049742c.
[43] Gaboriaud F, Dufrêne YF. Atomic force microscopy of microbial cells: application to nanomechanical properties, surface forces and molecular recognition forces. Colloids Surf B Biointerfaces 2007;54:10–9. http://dx.doi.org/10.1016/j.colsurfb.2006.09.014.
[44] Muller DJ. AFM: a nanotool in membrane biology. Biochemistry (Mosc) 2008;47:7986–98. http://dx.doi.org/10.1021/bi800753x.
[45] Shang L, Nienhaus K, Nienhaus GU. Engineered nanoparticles interacting with cells: size matters. J Nanobiotechnol 2014;12:b26.
[46] Bannunah AM, Vllasaliu D, Lord J, Stolnik S. Mechanisms of nanoparticle internalization and transport across an intestinal epithelial cell model: effect of size and surface charge. Mol Pharm 2014;11:4363–73. http://dx.doi.org/10.1021/mp500439c.
[47] Rozen Y, Belkin S. Survival of enteric bacteria in seawater. FEMS Microbiol Rev 2001;25:513. http://dx.doi.org/10.1111/j.1574-6976.2001.tb00589.x.
[48] Vital M, Hammes F, Egli T. *Escherichia coli* O157 can grow in natural freshwater at low carbon concentrations. Environ Microbiol 2008;10:2387–96. http://dx.doi.org/10.1111/j.1462-2920.2008.01664.x.
[49] Blaustein RA, Pachepsky Y, Hill RL, Shelton DR, Whelan G. *Escherichia coli* survival in waters: temperature dependence. Water Res 2013;47:569–78. http://dx.doi.org/10.1016/j.watres.2012.10.027.
[50] Daniel RA, Errington J. Control of cell morphogenesis in bacteria: two distinct ways to make a rod-shaped cell. Cell 2003;113:767–76.
[51] Alves CS, Melo MN, Franquelim HG, Ferre R, Planas M, Feliu L, et al. *Escherichia coli* cell surface perturbation and disruption induced by antimicrobial peptides BP100 and pepR. J Biol Chem 2010;285:27536–44. http://dx.doi.org/10.1074/jbc.M110.130955.
[52] Napierska D, Thomassen LC, Lison D, Martens JA, Hoet PH. The nanosilica hazard: another variable entity. Part Fibre Toxicol 2010;7:1.
[53] Capeletti LB, de Oliveira LF, Gonçalves K de A, de Oliveira JFA, Saito Â, Kobarg J, et al.. Tailored silica–antibiotic nanoparticles: overcoming bacterial resistance with low cytotoxicity. Langmuir 2014;30:7456–64. http://dx.doi.org/10.1021/la4046435.
[54] Wehling J, Volkmann E, Grieb T, Rosenauer A, Maas M, Treccani L, et al. A critical study: assessment of the effect of silica particles from 15 to 500 nm on bacterial viability. Environ Pollut 2013;176:292–9. http://dx.doi.org/10.1016/j.envpol.2013.02.001.
[55] Martínez-Castañón GA, Niño-Martínez N, Martínez-Gutierrez F, Martínez-Mendoza JR, Ruiz F. Synthesis and antibacterial activity of silver nanoparticles with different sizes. J Nanopart Res 2008;10:1343–8. http://dx.doi.org/10.1007/s11051-008-9428-6.
[56] Gammoudi I, Mathelie-guinlet M, Morote F, Beven L, Moynet D, Grauby-heywang C, et al. Morphological and nanostructural surface changes in *Escherichia coli* over time, monitored by atomic force microscopy. Colloids Surf B Biointerfaces 2016;141:355–64. http://dx.doi.org/10.1016/j.colsurfb.2016.02.006.
[57] Livadaru L, Kovalenko A. Fundamental mechanism of translocation across liquid-like membranes: toward control over nanoparticle behavior. Nano Lett 2006;6:78–83. http://dx.doi.org/10.1021/nl052073s.
[58] Yang L, Wang K, Tan W, He X, Jin R, Li J, et al. Atomic force microscopy study of different effects of natural and semisynthetic β-lactam on the cell envelope of *Escherichia c oli*. Anal Chem 2006;78:7341–5. http://dx.doi.org/10.1021/ac0604890.
[59] Leclère P, Rasmont A, Brédas JL, Jérôme R, Aimé JP, Lazzaroni R. Phase-separated microstructures in "all-acrylic" thermoplastic elastomers. Macromol Symp 2001;167:117–37. http://dx.doi.org/10.1002/1521-3900(200103)167:1<117::AID-MASY117>3.0.CO;2-1.
[60] Abraham T, Schooling SR, Beveridge TJ, Katsaras J. Monolayer film behavior of lipopolysaccharide from *Pseudomonas aeruginosa* at the air–water interface. Biomacromolecules 2008;9:2799–804. http://dx.doi.org/10.1021/bm800562r.
[61] Li A, Lee PY, Ho B, Ding JL, Lim CT. Atomic force microscopy study of the antimicrobial action of Sushi peptides on Gram negative bacteria. Biochim Biophys Acta BBA - Biomembr 1768;2007:411–8. http://dx.doi.org/10.1016/j.bbamem.2006.12.010.
[62] Meincken M, Holroyd DL, Rautenbach M. Atomic force microscopy study of the effect of antimicrobial peptides on the cell envelope of *Escherichia coli*. Antimicrob Agents Chemother 2005;49:4085–92. http://dx.doi.org/10.1128/AAC.49.10.4085-4092.2005.
[63] El Badawy AM, Silva RG, Morris B, Scheckel KG, Suidan MT, Tolaymat TM. Surface charge-dependent toxicity of silver nanoparticles. Environ Sci Technol 2010;45:283–7.
[64] Hartlen KD, Athanasopoulos APT, Kitaev V. Facile preparation of highly monodisperse small silica spheres (15 to > 200 nm) suitable for colloidal templating and formation of ordered arrays. Langmuir 2008;24:1714–20. http://dx.doi.org/10.1021/la7025285.
[65] Gaudon M, Basly B, Fauque Y, Majimel J, Delville MH. Thermochromic phase transition on $CuMo_{0.9}W_{0.1}O_4$@SiO_2 core shell particles. Inorg Chem 2009;48:2136–9. http://dx.doi.org/10.1021/ic802057c.
[66] Bolshakova AV, Kiselyova OI, Filonov AS, Frolova OY, Lyubchenko YL, Yaminsky IV. Comparative studies of bacteria with an atomic force microscopy operating in different modes. Ultramicroscopy 2001;86:121–8.